Article

Soil Genesis of Alluvial Parent Material in the Qinghai Lake Basin (NE Qinghai–Tibet Plateau) Revealed Using Optically Stimulated Luminescence Dating

Shuaiqi Zhang [1,2,3,4], Chongyi E [1,3,5,*], Xianba Ji [1,3,5], Ping Li [1,3,5], Qiang Peng [1,3,5], Zhaokang Zhang [1,3,5] and Qi Zhang [1,3,4]

1   Qinghai Province Key Laboratory of Physical Geography and Environmental Process, College of Geographical Science, Qinghai Normal University, Xining 810008, China; zshuaiqi@126.com (S.Z.); xianbaji2021@163.com (X.J.); lp1521469687@163.com (P.L.); pqiang0503@163.com (Q.P.); zzk199818@163.com (Z.Z.); zq15603786827@163.com (Q.Z.)
2   Qinghai Institute of Meteorological Science, Xining 810001, China
3   Key Laboratory of Tibetan Plateau Land Surface Processes and Ecological Conservation, Qinghai Normal University, Xining 810008, China
4   Qinghai Provincial Key Laboratory of Disaster Prevention and Reduction, Xining 810001, China
5   Academy of Plateau Science and Sustainability, People's Government of Qinghai Province and Beijing Normal University, Xining 810008, China
*   Correspondence: echongyi@163.com

Abstract: Alluvial parent material soil is an important soil type found on the Qinghai–Tibet Plateau (QTP) in China. However, due to the limited age data for alluvial soils, the relationship between alluvial geomorphological processes and soil pedogenic processes remains unclear. In this study, three representative alluvial parent material profiles on the Buha River alluvial plain in the Qinghai Lake Basin, northeast QTP, were analyzed using the optical luminescence (OSL) dating method. Combined with physical and chemical analyses of the soil, we further analyzed the pedogenic process of alluvial soil. The alluvial parent material of the Buha alluvial plain predominately yielded ages between 11.9 and 9.1 ka, indicating that the alluvial soil began to form during the early Holocene. The development of the alluvial soil on the first-order terrace presents characteristics of entisol with multiple burial episodes, mainly between 8.5 and 4.0 ka, responding to the warm and humid middle Holocene and high lake levels.

Keywords: Qinghai–Tibet Plateau; OSL dating; alluvial soil; soil genesis

1. Introduction

The soil of the Qinghai–Tibet Plateau (QTP) is critical for maintaining the ecological security of the plateau. Therefore, understanding the formation and evolution of this soil is necessary for reasonable soil conservation and sustainable utilization in the region. Preliminary analysis suggests that formation of the plateau soil is closely related to the input of aeolian dust, especially the development of meadow soil in mountainous areas [1–7]. The significant contribution of aeolian dust input in mountain soil formation has been reported worldwide [8,9].

Alluvial soil is widely developed on the vast lakeside and alluvial plains, which represent important components of the plateau soil. However, the formation and pedogenic processes of the alluvial soil have been rarely studied. Nevertheless, chronological information on alluvial soil is key to understanding the relationship between the relevant pedogenic process and climatic background. The pedogenic process can be simplified as a function of time and climate change with a minor contribution from topography, parental material, and vegetation. The well-documented paleoclimate record on the plateau provides an ideal data source for determining the climatic environment during the evolution

of the soil [10]. Therefore, our study seeks to determine the formation ages of the soils. In addition, studies of soil chronology can reveal the coupling processes underlying the accumulation of alluvial soil and the erosion of mountain soil.

The Qinghai Lake Basin is located in the northeastern part of the Qinghai–Tibet Plateau (Figure 1). Qinghai Lake, situated in the center of the basin, represents the largest inland saltwater lake in China. The northwestern part of the lake basin is dominated by alluvial–proluvial parent material types, which are mainly distributed on lakeside plains and floodplain landforms. Alluvium is a type of migration parent material composed of inorganic minerals [11]. Weathered detrital material is deposited after transportation via river flow, and soil formation initiates. Therefore, the alluvial material represents the parent material of the soil. Precise determination of the age of the parent material in the soil formation layer is of major importance, as it delineates the maximum age of the soil [4].
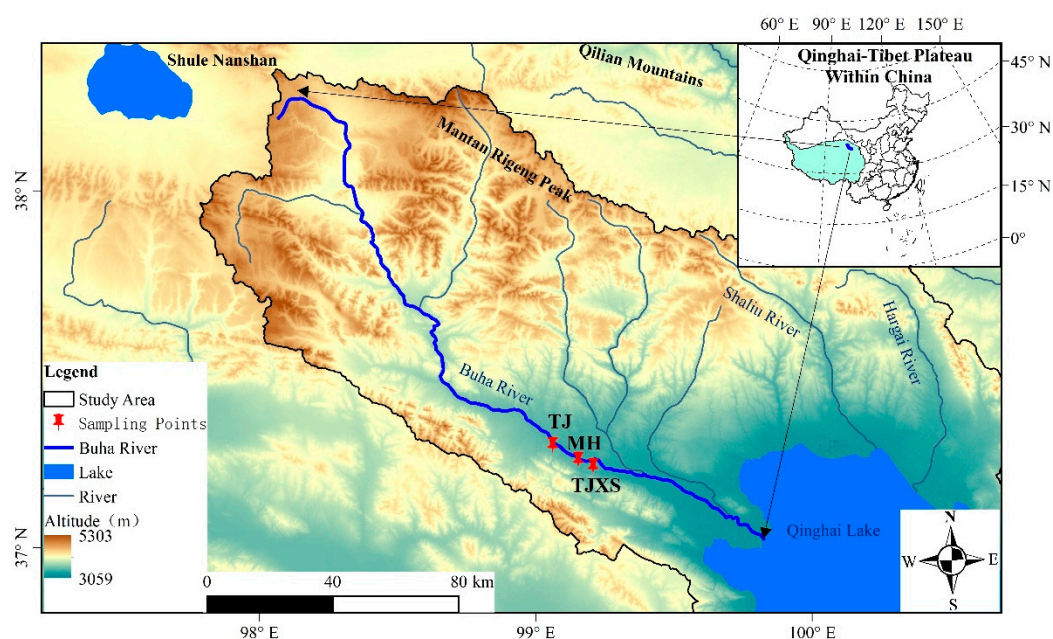

Figure 1. Sampling sites of alluvial parent soil in the Qinghai Lake Basin. The inset map shows the study area in the Qinghai–Tibet Plateau within China.

Previous studies found that optical stimulated luminescence (OSL) dating is suitable for measuring the alluvial and colluvium of rivers [12,13]. Previous studies have focused on the formation age of the alluvial fans around the Qinghai Lake Basin, providing a framework for the evolution of the basin. The age of the oldest dated alluvial–proluvial fan in the southern Qinghai Lake is about 38.8 ka [14]. However, the age of river alluvium in the northeast part of the lake may be older than 100 ka [15]. Samples from the eastern alluvial–proluvial profile were dated to about 102.5 ka [14]. The youngest age of the alluvial fan in the Qinghai Lake Basin is about 34–21 ka [16]. However, results on the age of alluvial parent soil in the Qinghai Lake Basin are still unclear. In this paper, we selected three representative profiles of alluvial soil for chronological analyses in the Buha River alluvial plain, the largest basin in the west of Qinghai Lake (Figure 1). Here, we combine chronological data with studies on the physical and chemical characteristics of the alluvial soil to reveal the pedogenic process of alluvial soil in the Qinghai Lake Basin.

2. Study Area

The Qinghai Lake Basin is located at an elevation of 3059–5303 m in the northeastern part of the Qinghai–Tibet Plateau, with an area of 29,661 km^2. This basin is a closed intermountain inland type, sloping from northwest to southeast. The relative height difference from the lake to the foothills is more than 2000 m, and the eroded structures, accumulation landforms, and aeolian geomorphology in this space developed as rings

with different widths. The Qinghai Lake Basin is characterized by a temperate semi-arid continental climate [17,18]. Gangcha weather station (1975–2011) located 10 km to the north of Qinghai Lake indicates that the area has an average annual temperature of −0.6 °C and total precipitation of 370 mm [5]. The main rivers in the basin include the Buha River, Shaliu River, and Hargai River (Figure 1). The Buha River, originating from the branch of the Qilian Mountains at the northern foot of the Mantan Rigeng Peak of Shule Nanshan, with the largest amount of water and the longest flow into Qinghai Lake, contributes about 54% of the total runoff and occupies 50% of the area in the Qinghai Lake Basin.

The Qinghai Lake Basin includes three uplift belt units—Datong Mountain, Nanshan Mountain, and Tuanbaoshan Riyue Mountain; three graben tectonic units—Buha River, Daotang River, and Ganzi River; and the Qinghai Lake fault basin [19]. According to geological investigations, the Buha River Basin is mainly composed of mountains with a combination of gneiss and quartz sandstone, with an alluvial plain landform type [20]. The soil types in the Qinghai Lake Basin mainly include alpine meadow soil, black calcareous soil, chestnut calcareous soil, grassland soil, sandy soil, desert soil, and saline soil. Different vegetation grows under different soil types and moisture conditions, and alpine meadows and grasslands are widely distributed within the watershed [21]. In addition, the water volume of Qinghai Lake is mainly supplied by rivers [22]. There are five rivers in the basin, namely Buha River, Shaliu River, Halgai River, Quanji River, and Heima River. Buha River and Shaliu River in the northwest provide the main water supply with large river runoff, accounting for 48.7% and 15.3% of Qinghai Lake's inflow [23].

3. Samples and Analytical Methods

Sample Profiles

The soil profile data of alluvial parent material investigated in our study were mainly sampled along the Buha River in the western Qinghai Lake Basin (Figure 1). This material was collected along three representative profiles at an average altitude of about 3300 m (Figure 2g). The soil samples exhibited characteristics of typical entisol and embryonic soil, with chestnut soil and meadow soil representing the main soil types. The Maohong (MH) and Tianjun (TJ) soil profiles were obtained from second-level alluvial–proluvial terraces of the Buha River. The Tianjun Xisha (TJXS) profile was samples on the first terrace of the Buha River (Table 1).

Figure 2. Photos of the profiles: (**a**) MH, (**b**) TJ, and (**c**) TJXS; geomorphic photos of the profiles: (**d**) MH, (**e**) TJ, and (**f**) TJXS; (**g**) satellite image data including the three soil profiles.

Table 1. Summary of studied soil profiles in the Qinghai Lake Basin.

Name	Latitude	Longitude	Altitude /m	Soil Type	Landform Type
Maohong	37.1934°	99.2251°	3346	Prototype soil	Alluvial–proluvial terraces (second-level terraces of the Buha River)
Tianjun	37.2559°	99.0807°	3384	Prototype soil	Alluvial–proluvial terraces (second-level terraces of the Buha River)
Tianjunxisha	37.2119°	99.1720°	3348	Entisol	First-level terraces of the Buha River

The Maohong profile (MH) is located on the second terrace of the Buha River (Figure 2d); the profile thickness of the whole layer is 50 cm. In addition, a 10 cm grass root system developed on the surface layer, followed by a grass mat layer. Sandy soil with 10 cm thickness at the lower part directly overlies the lower river gravel layer (Figure 2a), with thickness of almost 35 cm and grassroots distributed at different depths throughout the profile. A small amount of gravel intrusion occurs at a depth of 45 cm in the profile. A thick river gravel layer more than 5 m deep constitutes the lower part of the profile. OSL samples were collected at 15 cm, 30 cm, and 45 cm.

The Tianjun profile (TJ) is located on the second-level alluvial–proluvial terrace of the Buha River and has a thickness of 65 cm (Figure 2e). A grass mat layer is present in the uppermost 15 cm, and a humus layer occurs between 15 and 60 cm. The soil layer contains fine particles above 30 cm and more coarse particles below 30 cm. A thick alluvial–proluvial gravel layer constitutes the bottom of the profile. Three OSL samples were collected at intervals of 20 cm, and one additional OSL sample was collected from the lower sandy lens of the alluvial gravels (Figure 2b).

The entire soil profile of TJXS is exposed due to river erosion (Figure 2f). The thickness of the profile is about 138 cm, with multiple layers of river sand occurring in the middle section. The bottom of the profile is composed of a gravel layer (Figure 2c) 3 m higher than the modern river level. OSL samples were collected from the profile at 20 cm, 50 cm, 85 cm, 115 cm, and 136 cm.

4. Results

4.1. Luminescence Characteristics

OSL dating was carried out at the Laboratory of Qinghai Normal University after dating samples were pretreated under subdued red light. Quartz grain of 63–90 μm was extracted following the method of E et al. (2018) [24]. Quartz purity was assessed using an IR depletion ratio test (Duller, 2003) [25]. Equivalent doses (De) were determined via the single-aliquot regenerative-dose (SAR) protocol [26]. All De measurements were carried out on a standard Risø TL/OSL DA-20 reader [27]. The quartz OSL decay curve and growth curve for samples TJXS-1 are represented in Figure 3. Here, the quartz OSL signal quickly decreased to background noise in the first 2 s, indicating a fast component. We applied a preheating temperature of 240 °C for 10 s and a cut-heat temperature of 200 °C to determine De for the TJXS-1 sample (Figure 3). The decay curve and growth curves for the other two samples are presented in Appendix A.

Typically, 11–18 aliquots were measured for each sample, and the weighted mean De (with one standard error of uncertainty) was calculated. The rejection criteria were restricted via two test measurements (e.g., 0.9 < R5/R1 < 1.1 and R4/ N < 5%). The concentrations of U, Th, and K were determined with inductively coupled plasma mass spectrometry (ICP-MS) and converted to beta and gamma dose rates using the conversion factors reported by Guérin et al. (2012) [28]. The cosmic ray dose rate was calculated for each sample following the method of Prescott and Hutton (1994) [29]. An internal dose rate of 0.01 ± 0.002 Gy ka^{-1} was set based on the work of Vandenberghe and Tremblay (2008) [30]. The water content was assumed to be $15 \pm 7\%$ due to the samples' proximity to the river.
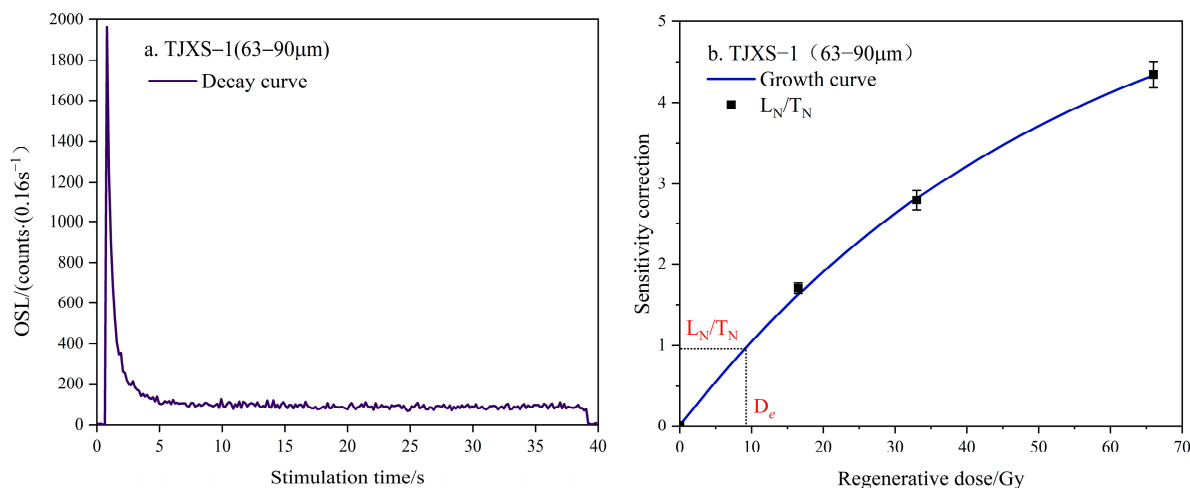
Figure 3. Decay curve and growth curve of the sample TJXS-1 (**a**,**b**).

4.2. OSL Dating of Alluvial Parent Material in the Qinghai Lake Basin

The age of the contact area between the bottom of the MH profile and the overlying gravel layer at a 40 cm depth is 11.9 ± 0.9 ka, indicating the formation of alluvium in the last deglacial period. The age of the soil at a 30 cm depth is 11.0 ± 1.1 ka, and the age of the soil near the surface (at a 15 cm depth) is ~1.6 ± 0.1 ka. These ages indicate a hiatus interval of about 9 ka at a depth of 30 to 15 cm.

The age at the contact point between the gravel layer and soil layer (60 cm depth) in the TJ profile is 10.0 ± 0.6 ka, and the lens of the underlying gravel layer (80 cm depth) is 10.5 ± 0.6 ka, indicating the almost simultaneous development of soil and alluvial deposition. The ages of the upper 20 cm grass mat layer and the 40 cm humus layer are 6.0 ka and 9.8 ka, respectively.

The ages of the TJXS profile are 3.9 ± 0.2 ka at a 20 cm depth, 6.2 ± 0.3 ka at an 85 cm depth, 8.5 ± 0.5 ka at a 115 cm depth, and 9.1 ± 0.6 ka at a 136 cm depth at the bottom of the profile. As the TJSX profile represents the variable characteristics of the sand and silt layer, all these OSL data for TJSX indicate different periods of alluvial soil formation (Table 2).

Table 2. Summary of the OSL dating results for alluvial parent soil in the Qinghai Lake Basin.

Sample No.	Depth /m	Th (ppm)	U (ppm)	K (%)	Dose Rate /(Gy/ka)	Particle Size /μm	Number /discs	D_e /Gy	Age /ka
MH1	0.15	13.7 ± 0.7	2.5 ± 0.4	1.7 ± 0.04	3.4 ± 0.15	63–90	17	5.4 ± 0.2	1.6 ± 0.1
MH2	0.3	12.4 ± 0.7	2.4 ± 0.4	1.6 ± 0.04	3.13 ± 0.14	63–90	16	34.7 ± 3.0	11.1 ± 1.1
MH3	0.45	11.9 ± 0.7	2.3 ± 0.4	1.6 ± 0.04	3.07 ± 0.14	63–90	14	36.5 ± 2.1	11.9 ± 0.9
TJ1	0.15	10.5 ± 0.7	2.4 ± 0.4	1.4 ± 0.03	2.87 ± 0.13	63–90	17	17.4 ± 0.4	6.1 ± 0.3
TJ2	0.3	11.4 ± 0.7	2.9 ± 0.4	1.5 ± 0.04	3.08 ± 0.14	63–90	18	30.3 ± 0.8	9.8 ± 0.6
TJ3	0.4	12.7 ± 0.7	3.5 ± 0.4	1.8 ± 0.04	3.53 ± 0.16	63–90	16	35.2 ± 1.2	10.0 ± 0.6
TJ4	0.6	17.6 ± 0.7	3.2 ± 0.4	2.2 ± 0.04	4.07 ± 0.18	63–90	17	42.7 ± 1.3	10.5 ± 0.6
TJXS1	0.2	10.0 ± 0.7	2.6 ± 0.4	1.7 ± 0.03	3.1 ± 0.14	63–90	17	12.1 ± 0.3	3.9 ± 0.2
TJXS2	0.85	8.7 ± 0.6	2.0 ± 0.3	1.6 ± 0.03	2.71 ± 0.12	63–90	17	16.8 ± 0.5	6.2 ± 0.3
TJXS3	1.15	12.7 ± 0.7	2.0 ± 0.3	1.9 ± 0.04	3.24 ± 0.14	63–90	11	27.5 ± 1.2	8.5 ± 0.5
TJXS4	1.36	15.3 ± 0.8	2.2 ± 0.4	2.2 ± 0.04	3.46 ± 0.16	63–90	16	31.4 ± 1.7	9.1 ± 0.7

4.3. Soil Grain Size and Organic Matter Content Analyses

The studied soil samples possess typical alluvial characteristics according to the results of the particle size measurements. These soils are mainly composed of sand and silt, with the grain sizes varying significantly at different depths and in different sedimentary strata. Notably, the samples comprised 72.6% sand (Figure 4). The results of the three types of soil particle size distribution curves are shown in Figure 5. Here, the soil particle size curves of the MH and TJ profiles are basically consistent, showing a bimodal distribution, with the main peak mainly concentrated at 50 μm. The soil particle size curve of the TJXS profile

also shows a bimodal distribution but varies with high frequency and amplitude. The main peak particle size is concentrated at 900 µm, indicating strong hydrodynamic conditions.

The median particle size of the MH profile shows a significant upward trend, with a decrease in organic matter content. At a depth of 20–30 cm, the median particle size of the TJ profile slightly decreases, while the organic matter content shows an opposite trend to the average particle size curve. The median particle size of the TJXS profile ranges from 12 to 215 µm, with an average value of 79.1 µm. The soil organic matter content of TJSX ranges from 16.1 to 45.6 g/kg—much higher than that of MH and TJ—with a slight increase from the bottom to the surface (Figure 5).
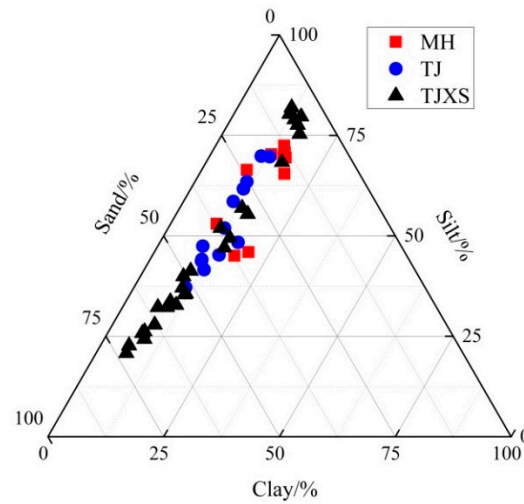

Figure 4. Distribution of grain sizes of the alluvial parent soil in the studied profiles of the Qinghai Lake Basin.
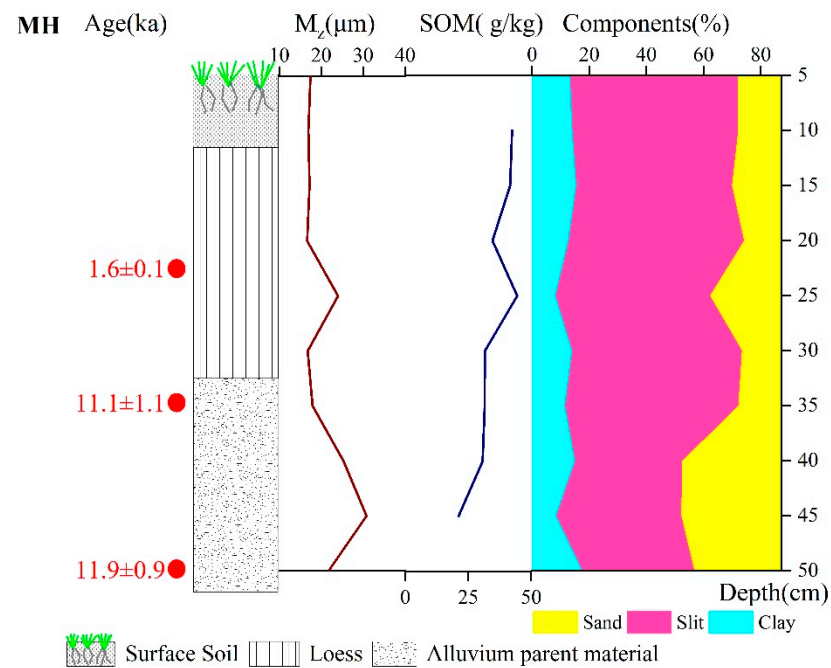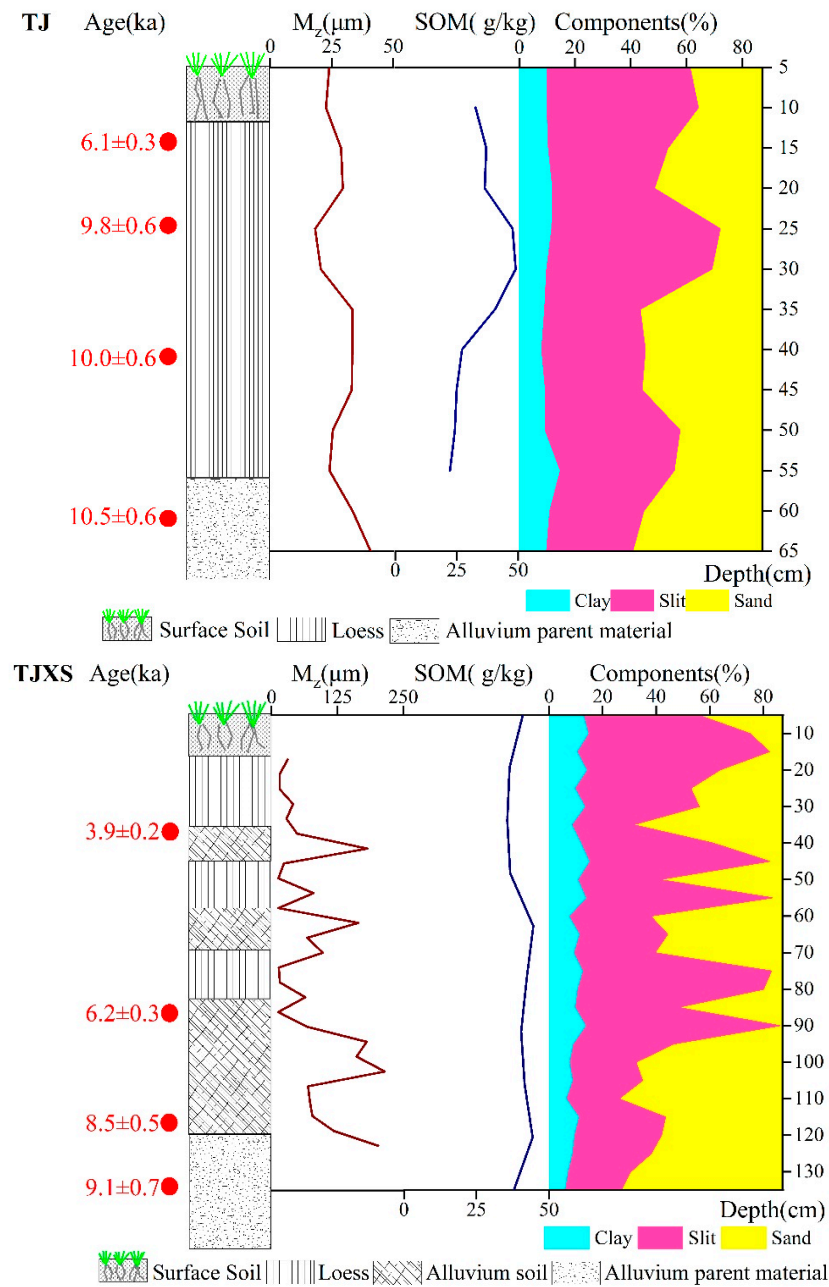

Figure 5. *Cont.*

Figure 5. Schematic diagram of the soil's genetic layers, including age, average particle size, organic matter content, and component content in the MH, TJ, and TJXS profiles.

5. Discussion

The OSL ages of alluviums from different soil profiles reflect the formation age of the alluvial parental materials (Figure 5), indicating the maximum age of the alluvial soil formation. All of the studied soil profiles formed during the Holocene. The initial age of alluvial soil was concentrated in the early Holocene (9.1–11.9 ka). Here, the initial OSL ages of the TJ (10.5 ka) and MH (11.9 ka) profiles on the second terrace are slightly older than the age of TJSX (9.1 ka) on the first terrace. Thus, the general fluvial geomorphological process should be mainly controlled while considering the base level of erosion, i.e., the Qinghai Lake level.

The lake level of Qinghai Lake in the Early Holocene was about 10 m lower than the modern lake level [31]. Moreover, the drop of the erosion base promoted the erosion of upstream materials. During this time, the Buha River was dominated by downcutting,

with the gravel stratum indicating a high-energy environment and strong hydrodynamic conditions. As the river cut through and formed river terraces or exposed land surfaces, vegetation started to grow on the alluvium, which serves as the initial soil-forming parent material in the process of soil pedogenesis. However, with the subsequent increase in vegetation cover, the accumulation of abundant aeolian dust material on the plateau became the dominant soil formation process. The second terrace is 10 m higher than the first, making it difficult for the Buha River to impact. Thus, the alluvial process changed to an aeolian sand and atmospheric dust deposition process. The striking similarities in soil grainsize between the upper soils and dust fall indicate that the upper soil was mainly developed through aeolian dust accumulation, which is consistent with the results of previous studies in the Three River Source Region on the plateau [7]. However, the relatively low SOM content likely indicates weak pedogenic intensity; the temperature increased with relatively high-frequency and -amplitude oscillations and there were strong aeolian activities during the early Holocene. During the middle Holocene, the temperature remained relatively high and stable, with the weakest aeolian activities and intensified pedogenesis. During the late Holocene, the temperature decreased at a relatively high amplitude, with renewed aeolian activities and weak pedogenesis [10,32]. The climatic system exhibits greater complexity in the Qinghai Lake Basin, situated at the periphery of the East Asian Summer Monsoon and the Indian Summer Monsoon influences, as compared to other sectors of the Qinghai–Tibet Plateau [33]. Therefore, we propose that the end of the last deglacial period and the early stage of the Early Holocene represented major formation periods for alluvial parental material in the alluvial plain of the Buha River.

However, during the middle Holocene, the Qinghai Lake level gradually increased from ~8 ka to ~10 m higher than the modern lake by ~6 ka [31,34]. The rise in the erosion base level diminished the downcutting erosion ability of the Buha River, with the dominant mode being lateral erosion. The TJXS profile on the first-order terrace indicates frequent increases in sand content but fewer gravel and silt-sandwiched sand layers (Figure 6), indicating a relatively low-energy environment and weak hydrodynamic conditions. Soils frequently developed on these alluviums and were buried by subsequently deposited alluvial materials. The river sand exposed to the surface was nutrient-rich soil, directly supporting the growth of vegetation. Vegetation serves as a natural dust collector and captures silt-sized dust. Subsequently, another stronger fluvial event occurred with alluvial deposition, burying the previously developed soil. Until the height of the soil profile became high enough that the Buha River could not wash across the riverbanks, alluvium was not deposited. However, aeolian dust was continuously deposited during this period. In the TJSX profile, frequent alluvial deposition occurred during 8.5–4.0 ka. At least three layers of paleosols developed from this alluvium, responding to the rising lake level and warm–wet climate conditions [18,31,32,34–42]. The remarkably high SOM content in TJSX indicates high vegetation productivity during the middle Holocene, suggesting an intensified pedogenic period. Therefore, the middle Holocene would have represented a significantly intensified developmental period for alluvial soils. The magnetic susceptibility of aeolian dust is a sensitive proxy for soil development and also indicates intensified soil development in Qinghai lake during 8.5–4.0 ka [32]. Figure 7C shows the intensity variation of the East Asian summer monsoon, indicating a stronger EASM from ~8 to 3 ka and the maximum monsoon (30% higher precipitation than present) from ~7.8 to 5.3 ka [39,43,44], which is consistent with the timing of alluvial soil development. The increased frequency of palaeosol indicates intensified soil development from ~8.6 to 3.2 ka in the Chinese Loess Plateau [45]. This intensified soil development based on different parent materials was mainly concentrated during the middle Holocene, indicating that climate was the dominant factor in soil development, rather than the parent material or landform.
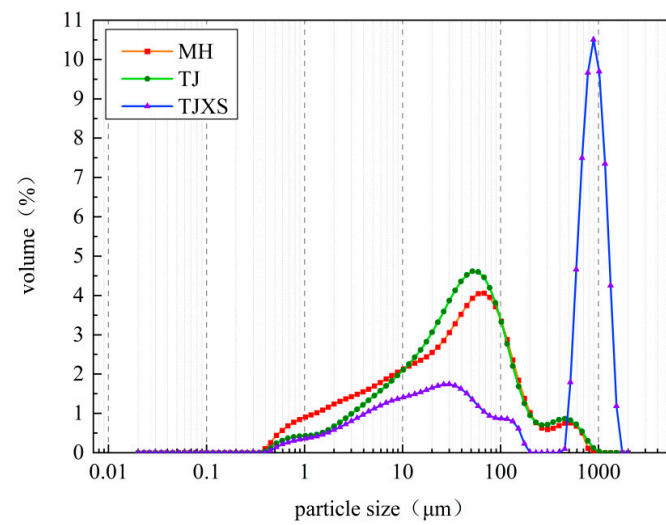
Figure 6. Distribution characteristics of soil particle size in MH, TJ, and TJXS upper profiles.
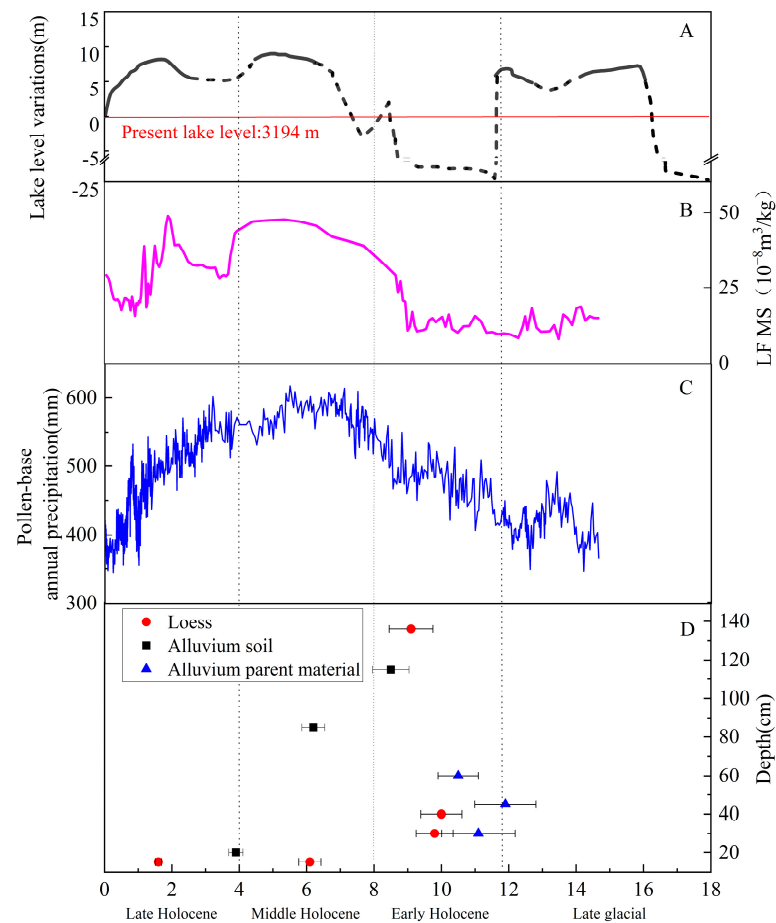

Figure 7. (**A**) Reconstructed lake level based on the paleoshoreline [31] and (**B**) the low-frequency magnetic susceptibility (LFMS) of the ND profile, Qinghai Lake [32]; (**C**) the high seas precipitation records based on pollen [42]; (**D**) the age of sand, alluvial soil, and alluvial parent materials within the three profiles.

The median grain size in the TJ and MH profiles is primarily composed of medium silt, which is much finer than silt in the TJSX profile. The grain size frequency distribution curves in the TJ and MH profiles resemble the atmospheric dust fall at Xiaobohu station in the eastern portion of Qinghai Lake [4,46]. This result indicates that the soils on second terrace of Buha River mainly follow the "wind dust accretion type" mode on the upper profile [4–6]. The bottom soils on the second terrace and top soil on the first terrace represent an "alluvial parent material with aeolian dust accumulation" type, which is similar to the alpine meadow soil in the Three River Source Region [7].

The similarities show that the upper soil mainly developed via the accumulation of aeolian dust, consistent with previous studies. This process followed a "wind dust accretion type" mode of accumulation [4,5,31]. Based on the early alluvial process, the soil formation mode of alluvial soil in Qinghai Lake represents an "alluvial parent material with aeolian dust accumulation" type, similar to that of the alpine meadow soil in the Three River Source Region studied by Xianba et al., 2022 [7] (Figure 7).

6. Conclusions

Fluvial geomorphological processes and fluctuations in the lake level have important impacts on the formation of alluvial soil and pedogenesis processes in the Qinghai Lake Basin. The initial formation age of the alluvial parent material in the Qinghai Lake Basin is between 11.9 and 9.1 ka, while the formation ages of the alluvial soil are concentrated between 8.5 and 4.0 ka. Most alluvial soils formed during the middle Holocene.

1. The alluvial parent material in the Qinghai Lake Basin was buried several times during the middle Holocene, which was affected by the warm and wet climatic condition during that period. Soil pedogenesis and humus accumulation during 8.5–4 ka were relatively strong in response to the high lake levels.
2. The underlying alluvial parent material is characteristic of typical fluvial sediment and mainly composed of gravel and river sand components, while the upper soil is characteristic of wind dust. Therefore, alluvial soils followed the "alluvial parent material with aeolian dust accumulation mode" in the Qinghai Lake Basin.

The Qinghai Lake Basin covers a vast area and has many types of parent materials. However, the content of this study is limited. Only the typical alluvial parent material types in the Buha River basin were studied, with minimal consideration of age or the physical and chemical properties of other types of parent materials. In addition, few profiles have been considered. In future research, we should collect and study other different types of parent material profiles in the Qinghai Lake basin.

Author Contributions: Conceptualization, C.E.; methodology, C.E.; software, S.Z.; validation, X.J.; formal analysis, Q.P.; investigation, P.L.; resources, Q.Z.; data curation, X.J.; writing—original draft preparation, S.Z.; writing—review and editing, C.E.; visualization, Z.Z.; supervision, Z.Z. All authors have read and agreed to the published version of the manuscript.

Institutional Review Board Statement: Not applicable.

Informed Consent Statement: Not applicable.

Data Availability Statement: The data presented in this study are available on request from the corresponding author. The data are not publicly available due to privacy.

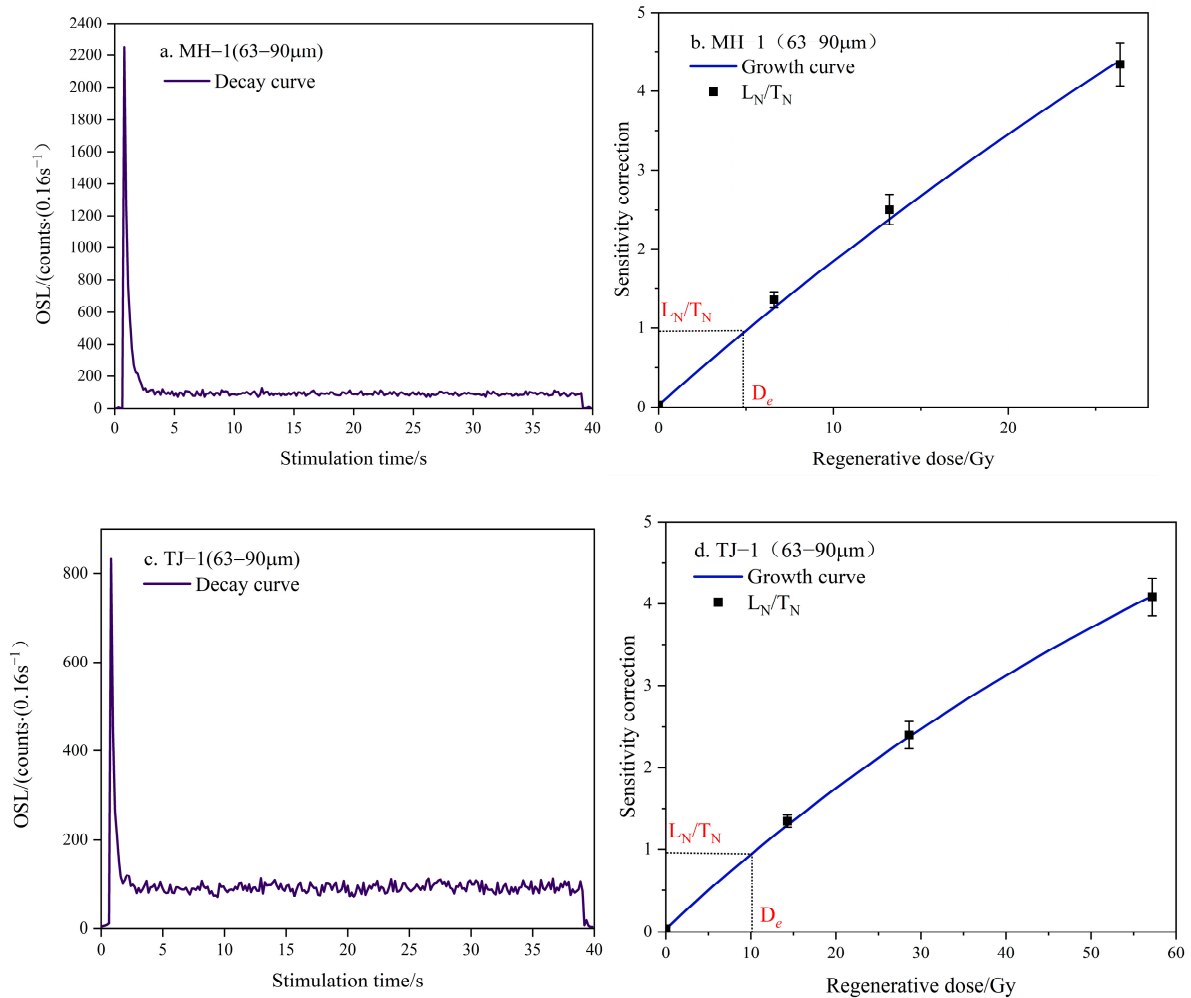**Conflicts of Interest:** The authors declare no conflicts of interest.

Appendix A

Figure A1. Decay curve and growth curve of samples MH-1 (**a**,**b**) and TJ-1 (**c**,**d**).

References

1. Feng, J.L.; Hu, H.P.; Chen, F. An eolian deposit–buried soil sequence in an alpine soil on the northern Tibetan Plateau: Implications for climate change and carbon sequestration. *Geoderma* **2016**, *266*, 14–24. [CrossRef]
2. Yang, F.; Zhang, G.L.; Yang, F.; Yang, R.M. Pedogenetic interpretations of particle-size distribution curves for an alpine environment. *Geoderma* **2016**, *282*, 9–15. [CrossRef]
3. Yang, F.; Zhang, G.L.; Sauer, D.; Yang, F.; Yang, R.M.; Liu, F.; Yang, J.L. The geomorphology–sediment distribution–soil formation nexus on the northeastern Qinghai-Tibetan Plateau: Implications for landscape evolution. *Geomorphology* **2020**, *354*, 107040. [CrossRef]
4. Zhang, J.; Chongyi, E.; Wu, C.; Sun, Y.; Li, P.; Shi, Y.; Sun, M. An alpine meadow soil chronology based on OSL and radiocarbon dating, Qinghai Lake, northeastern Tibetan Plateau. *Quat. Int.* **2020**, *562*, 35–45. [CrossRef]
5. E, C.Y.; Zhang, J.; Wu, C.Y.; Sun, Y.J.; Sun, M.P.; Yan, W.T.; Lv, S.C. Study of Chronology of the Meadow Soil in the Qinghai Lake Basin by Means of Optically Stimulated Luminescence. *Acta Pedol. Sin.* **2018**, *55*, 1325–1335, (In Chinese with English Abstract)
6. Lin, Y.C.; Feng, J.L.; Zhang, J.F.; Ju, J.T.; Hu, Z.G.; Gao, S.P. Origin of Parent Materials and Pedogensis for Alpine Meadow Soils in Amdo, Northern Tibetan Plateau. *J. Mt. Sci.* **2012**, *30*, 709–720, (In Chinese with English Abstract)
7. Xian, B.; E, C.Y.; Sun, M.P.; Zhang, J.; Zhang, S.; Xie, L. Formation age and causes of alpine meadow soil in Three River Headwater Region based on Optically Stimulated Luminescence dating. *Bull. Soil Water Conserv.* **2022**, *42*, 158–165, (In Chinese with English Abstract)
8. Grant, J.P.; Barker, J.C. The Harvard Research: Genesis to Exodus and Beyond. *Xinjiang Farm Res. Sci. Technol.* **2007**, *3*, 49.
9. Prins, M.A.; Vriend, M.; Nugteren, G.; Vinther, J.; Lu, H.; Zheng, H.; Weltje, G.J. Late Quaternary aeolian dust input variability on the Chinese Loess Plateau: Inferences from unmixing of loess grain-size records. *Quat. Sci. Rev.* **2007**, *26*, 230–242. [CrossRef]

10. Peng, Q.; E, C.; Li, X.; Sun, Y.; Zhang, J.; Zhang, S.; Shi, Y.; Ji, X.; Zhang, Z. Holocene Paleoclimate Changes around Qinghai Lake in the Northeastern Qinghai-Tibet Plateau: Insights from Isotope Geochemistry of Aeolian Sediment. *Atmosphere* **2024**, *15*, 833. [CrossRef]

11. Li, X.; Liu, W.; Xu, L. Evaluation of lacustrine organic δ13C as a lake-level indicator: A case study of Lake Qinghai and the satellite lakes on the Tibetan Plateau. *Palaeogeogr. Palaeoclimatol. Palaeoecol.* **2019**, *532*, 109274. [CrossRef]

12. Eriksson, M.G.; Christiansson, C. Accelerated soil erosion in central Tanzania during the last few hundred years. *Phys. Chem. Earth* **1997**, *22*, 315–320. [CrossRef]

13. Olley, J.M.; Caitcheon, G.G.; Roberts, R.G. The origin of dose distributions in fluvial sediments, and the prospect of dating single grains from fluvial deposits using optically stimulated luminescence. *Radiat. Meas.* **1999**, *30*, 207–217. [CrossRef]

14. Madsen, D.B.; Haizhou, M.; Rhode, D.; Brantingham, P.J.; Forman, S.L. Age constraints on the late Quaternary evolution of Qinghai Lake, Tibetan Plateau. *Quat. Res.* **2008**, *69*, 316–325. [CrossRef]

15. Rhode, D.; Haizhou, M.; Madsen, D.B.; Brantingham, P.J.; Forman, S.L.; Olsen, J.W. Paleoenvironmental and archaeological investigations at Qinghai Lake, western China: Geomorphic and chronometric evidence of lake level history. *Quat. Int.* **2010**, *218*, 29–44. [CrossRef]

16. Long, H.; Tsukamoto, S.; Buylaert, J.P.; Murray, A.S.; Jain, M.; Frechen, M. Late Quaternary OSL chronologies from the Qinghai Lake (NE Tibetan Plateau): Inter-comparison of quartz and K-feldspar ages to assess the pre-depositional bleaching. *Quat. Geochronol.* **2019**, *49*, 159–164. [CrossRef]

17. Chen, F.; Wu, D.; Chen, J.; Zhou, A.; Yu, J.; Shen, J.; Wang, S.; Huang, X. Holocene moisture and East Asian summer monsoon evolution in the northeastern Tibetan Plateau recorded by Lake Qinghai and its environs: A review of conflicting proxies. *Quat. Sci. Rev.* **2016**, *154*, 111–129. [CrossRef]

18. Liu, J.; Cai, Y.J.; Wang, J. Soil classification of Qinghai Lake basin based on remote sensing, Remote Sensing for Land and Resources. *Remote Sens. Land Resources*, 2014; 26, 57–62.

19. Bian, Q.T.; Liu, J.Q.; Luo, X.Q.; Xiao, J. Geotectonic Setting, Fomation and Evolution of the Qinghai Lake. *Seismol. Geol.* **2000**, *22*, 20–26.

20. Ma, R.J. Record of physical geography investigation around Qinghai Lake. *J. Northwest Norm. Univ. (Nat. Sci.)* **1982**, 41–57.

21. Li, X.Y.; Xu, H.Y.; Sun, Y.L.; Zhang, D.S.; Yang, Z.P. Lake-Level Change and Water Balance Analysis at Lake Qinghai, West China during Recent Decades. *Water Resour. Manag.* **2007**, *21*, 1505–1516. [CrossRef]

22. Shu, W.X.; Li, S.J.; Liu, J.F. Simulation of water change in Qinghai Lake and affection factors. *Arid. Land Geogr.* **2008**, *31*, 229–236.

23. Yi, W.J.; Li, X.Y.; Cui, B.L.; Ma, Y.J. Climate Change and Impact on Water Level of the Qinghai Lake Watershed. *J. Arid. Meteorol.* **2010**, *28*, 375–383.

24. E, C.Y.; Sohbati, R.; Murray, A.S.; Buylaert, J.P.; Liu, X.; Yang, L.; Yuan, J.; Yan, W. Hebei loess section in the Anyemaqen Mountains, northeast Tibetan Plateau: A high-resolution luminescence. *Boreas* **2018**, *47*, 1170–1183. [CrossRef]

25. Duller, G.A.T. Distinguishing quartz and feldspar in single grain luminescence measurements. *Radiat. Meas.* **2003**, *37*, 161–165. [CrossRef]

26. Murray, A.S.; Wintle, A.G. Luminescence dating of quartz using an improved single-aliquot regenerative-dose protocol. *Radiat. Meas.* **2000**, *32*, 57–73. [CrossRef]

27. Bøtter-Jensen, L.; Thomsen, K.J.; Jain, M. Review of optically stimulated luminescence (OSL) instrumental developments for retrospective dosimetry. *Radiat. Meas.* **2010**, *45*, 253–257. [CrossRef]

28. Guérin, G.; Mercier, N.; Nathan, R.; Adamiec, G.; Lefrais, Y. On the use of the infinite matrix assumption and associated concepts: A critical review. *Radiat. Meas.* **2012**, *47*, 778–785.

29. Prescott, J.R.; Hutton, J.T. Cosmic ray contributions to dose rates for luminescence and ESR dating: Large depths and long-term time variations. *Radiat. Meas.* **1994**, *23*, 497–500. [CrossRef]

30. Vandenberghe, C.; Tremblay, M. The role of pay satisfaction and organizational commitment in turnover intentions: A two-sample study. *J. Bus. Psychol.* **2008**, *22*, 275–286. [CrossRef]

31. Liu, X.J.; Lai, Z.; Madsen, D.; Zeng, F. Last deglacial and Holocene lake level variations of Qinghai Lake, north-eastern Qinghai–Tibetan Plateau. *J. Quat. Sci.* **2015**, *30*, 245–257. [CrossRef]

32. E, C.Y.; Zhang, J.; Cheng, Z.Y.; Sun, Y.J.; Zhao, Y.J.; Li, P.; Sun, M.P.; Shi, Y.K. High resolution OSL dating of aeolian activity at Qinghai Lake, Northeast Tibetan Plateau. *Catena* **2019**, *183*, 104180.

33. Li, X.; Liu, X.; He, Y.; Liu, W.; Zhou, X.; Wang, Z. Summer moisture changes in the Lake Qinghai area on the northeastern Tibetan Plateau recorded from a meadow section over the past 8400 yrs. *Glob. Planet. Chang.* **2018**, *161*, 1–9. [CrossRef]

34. Yu, J.Q. Lake Qinghai, China: A Multi-Proxy Investigation on Sediment Cores for the Reconstructions of Paleoclimate and Paleoenvironment Since the Marine Isotope Stage 3. Ph.D. Thesis, Faculty of Materials and Geoscience, Technical University of Darmstadt, Darmstadt, Germany, 2005.

35. Hou, G.L.; Wei, H.C.; E, C.Y.; Sun, Y. Human activities and environmental change in Holocene in the northeastern margin of Qinghai-Tibet Plateau: A case study of JXG2 relic site in Qinghai Lake. *Acta Geogr. Sin.* **2013**, *68*, 9. [CrossRef]

36. Kaufman, D.; McKay, N.; Routson, C.; Erb, M.; Dätwyler, C.; Sommer, P.S.; Heiri, O.; Davis, B. Holocene global mean surface temperature, a multi-method reconstruction approach. *Sci. Data* **2020**, *7*, 201. [CrossRef]

37. Rhode, D. Wood Charcoal from Archaeological Sites in the Qinghai Lake Basin, Western China: Implications for Human Resource Use and Anthropogenic Environmental Change. *J. Ethnobiol.* **2016**, *36*, 571–594. [CrossRef]

38. Xu, C.X.; E, C.Y.; Shi, Y.K.; Zhang, J.; Sun, M.P.; Zhang, Z.K.; Zeng, Y.X. Holocene Aeolian Activity Recorded by Mountain Paleosols, Gonghe Basin, Northeast Qinghai-Tibet Plateau. *Front. Earth Sci.* **2022**, *10*, 832993. [CrossRef]

39. Dong, Y.; Wu, N.; Li, F.; Zhang, D.; Zhang, Y.; Shen, C.; Lu, H. The Holocene temperature conundrum answered by mollusk records from East Asia. *Nat. Commun.* **2022**, *13*, 5153. [CrossRef] [PubMed]

40. Stott, L.; Cannariato, K.; Thunell, R.; Haug, G.H.; Koutavas, A.; Lund, S. Decline of surface temperature and salinity in the western tropical Pacific Ocean in the Holocene epoch. *Nature* **2004**, *431*, 56–59. [CrossRef]

41. Vinther, B.M.; Buchardt, S.L.; Clausen, H.B.; Dahl-Jensen, D.; Johnsen, S.J.; Fisher, D.A.; Koerner, R.M.; Raynaud, D.; Lipenkov, V.; Andersen, K.K.; et al. Holocene thinning of the Greenland ice sheet. *Nature* **2009**, *461*, 385–388. [CrossRef]

42. Zhang, W.; Wu, H.; Geng, J.; Cheng, J. Model-data divergence in global seasonal temperature response to astronomical insolation during the Holocene. *Sci. Bull.* **2022**, *67*, 25–28. [CrossRef]

43. Chen, F.; Xu, Q.; Chen, J.; Birks, H.J.B.; Liu, J.; Zhang, S.; Jin, L.; An, C.; Telford, R.J.; Cao, X.; et al. East Asian summer monsoon precipitation variability since the last deglaciation. *Sci. Rep.* **2015**, *5*, 11186. [CrossRef]

44. Chen, F.; Duan, Y.W.; Hao, S.; Chen, J.; Feng, X.; Hou, J.; Cao, X.; Zhang, X.; Zhou, T. Holocene temperature major warm period model and continuous warming model: Record-model comparison problem and research prospects. *Sci. China Earth Sci.* **2023**, *53*, 1699–1717. (In Chinese)

45. Wang, H.; Chen, J.; Zhang, X.; Chen, F. Palaeosol development in the Chinese Loess Plateau as an indicator of the strength of the East Asian summer monsoon: Evidence for a mid-Holocene maximum. *Quat. Int.* **2014**, *334*, 155–164. [CrossRef]

46. E, C.Y.; Xi, Y.S.; Sun, Y.J.; Zhao, Y.J.; Yang, L.; Lv, S.C. Dust Flux and Grain Size Variation Analysis in Northeast Qinghai-Tibet Plateau. *J. Salt Lake Res.* **2016**, *24*, 62–74, (In Chinese with English Abstract)